Investigation of the Processability of Polyether Block Amide in High Speed Sintering

Marco Wimmer*†, Jan Kemnitzer*, David Förster†, Johann Schorzmann† and
Frank Döpper*†

* Fraunhofer Institute for Manufacturing Engineering and Automation IPA,
Universitaetsstrasse 9, 95447 Bayreuth, Germany
† Chair of Manufacturing and Remanufacturing Technologies, University of Bayreuth,
Universitaetsstrasse 30, 95447 Bayreuth, Germany

Abstract

The High Speed Sintering (HSS) process ranks among the processes of Powder Bed Fusion of polymers (PBF-P) of Additive Manufacturing (AM). Its scalability, constant layer time and high quality of complex parts compared to other AM processes are some of the characteristics of the HSS showing its potential for series production for small to medium series. Most of the investigations for the PBF-P processes were conducted using commercially available materials like Polyamide 12 (PA12), Polyamide 6 (PA6), Thermoplastic polyurethane (TPU), Polypropylene (PP) and Polybutylene terephthalate (PBT). This work reports from the processing of Polyether block amide (PEBA) in HSS. As a block-copolymer on amide basis, PEBA shows higher performance compared to other block-copolymers like TPU: The high elastic properties, low density and high service temperature make PEBA an ideal material for the use in the athletic footwear and outdoor industry. Until now, no research was conducted on processing PEBA powder in HSS. This work focusses on the material analysis of PEBA powder and manufacturing of specimens of varying sets of process parameters using methods of Design of Experiments (DoE) and IFINAM TPA powder from Evonik. Based on a predictive model, parameter sets for optimum mechanical properties, dimensional accuracy and overall part properties of HSS PEBA parts were optimised within the framework of this work.

Introduction

The High Speed Sintering (HSS) process ranks among the Powder Bed Fusion of Polymers (PBF-P) of Additive Manufacturing (AM) [1]. Unlike the Laser Sintering (LS) process, where the selective energy input into the polymer powder bed is given by a laser, the HSS process combines inkjet printing of an infrared absorbing ink, using carbon black as radiation absorbing material (RAM) and an infrared sintering lamp [2]. The type of selective energy input determines the process category within the AM. According to DIN EN ISO 52900, HSS ranks among the process category of powder bed fusion with infrared radiation of polymers (PBF-IR/P) [1]. The two-dimensional application of RAM and radiation with a sintering lamp in HSS yield great potential regarding scalability and range of polymer materials compared to the selective energy input in LS. Due to the longer lasting and more gentle selective energy input into the polymer powder, viscous polymers like Thermoplastic urethane (TPU) are given more time to sinter and higher recycling rates can be achieved compared to LS. [3]

Most of the research using HSS was done using semicrystalline thermoplastics like Polyamide 12 (PA12) [4–18], Polypropylene (PP) [19,20], Polyamide 11 [21] and Polyethylene terephthalate [22]. Regarding Thermoplastic Elastomers (TPEs), an elastomeric form of Nylon [12] and TPE without mentioning of the molecular basis [23–25] was used in HSS.

Polyether block polyamide (PEBA) is a class of TPE, more precisely a block-copolymer with high costs but high performance [26]. The polymer chains of block-copolymer TPEs like TPU or PEBA consist of alternating hard and soft segments. For PEBA, amide linkages are connecting the soft and hard segments, which have a higher resistance to chemical hydrolysis than urethane linkages. The ratio of soft elastic and hard thermoplastic segments determine the properties, like the elastomer´s hardness (60 Shore A to 65 Shore D) [27]. The hard segments affect the processing and melting point of the PEBA. Compared to other TPEs, PEBA can reach the highest service temperatures of up to 170 °C. [28,29]

Due to its lower density and elevated chemical resistance, strength and toughness, elastic recovery, damping capacity and sterilizability compared to other TPEs, PEBA is used for automotive, aerospace, sportswear and medical applications like sports shoes, ski boots, ski goggles and catheters [26,27].

Most of the conducted research was done using commercially available PEBA for injection moulding and focused on the analysis of the general material properties. Regarding the HSS process, only Williams et al. [30] conducted research examining the wettability of polymer powders and part colour of PA12, PP, PA11, PA12 and PEBA printed parts. This work focusses on the suitability and processability of PEBA powder within the HSS and the effect of process parameters on mechanical and geometric properties of HSS printed PEBA parts.

Materials and Methods

The PEBA Powder

The investigations carried out in this work were performed using INFINAM TPA, a PEBA powder from Evonik. A Micrometrics Accu Pyc II 1340 was used to measure the solid density ρ_F of virgin (unsieved) and used (sieved with a mesh size of 180 µm) PEBA powder material according to (DIN 66137-1) using pycnometry and helium gas to determine the maximum achievable density of HSS parts made from this PEBA. After flooding the measuring chamber 10 times, each powder sample was measured 10 times using a filling pressure of 135.45 kPag. To obtain the particle size distributon (PSD), dynamic image analisys according to ISO 13322-2 was done using a Retsch Technology Camsizer XT. By using the X-Jet module with a dispersing pressure of 70.0 kPa and a gap width of 4.0 mm, virgin and used PEBA powder was examined to classify the particle sizes from 0.0 µm to 200.0 µm in steps of 2.5 µm. The volume based PSD curves were evaluated according to DIN ISO 9276. Dynamic scanning calorimetry (DSC) was done for virgin and used PEBA powder between 25°C and 180°C with a heating and cooling rate of 10 K/min to derive the melting temperature, crystallisation temperature and the sintering window from the heating and cooling curves. Before manufacturing parts with the PEBA powder, a Russell Finex Minisifter vibration sieve with a mesh size of 180 µm was used to sieve virgin and used powder. Parts were manufactured using a mixture of used/virgin powder in a ratio of 70/30, mixed within a Dr. Fritsch PM10 for 30 minutes with a rotation speed of 48 min⁻¹.

The HSS Machine

Figure 1 shows the build chamber of the voxeljet AG VX200 HSS 'beta version', used to manufacture HSS PEBA parts. The overhead lamp (① in Figure 1), containing six ceramic radiators, was used to reach the selected process temperature and to maintain a homogenous temperature distribution on the powder bed surface. The build box (② in Figure 1), consisted of an in z-direction vertically moveable and heatable floor plate, surrounded by four seperately heatable side walls. The dimensions of the build box were 290 mm in x-, 140 mm in y-, and 180 mm in z-direction, which resulted in a maximum build volume of 7.308 cm³.

The layer thickness is defined by the stroke of the floor plate in negative z-direction. A double walled, fluid-heated, custom recoater (③ in Figure 1) flooded with heat resistant silicone oil and heated by a Huber Ministat 230 was used to apply each layer of PEBA powder using a vibrating blade system. The powder output was determined by the recoater gap, the intensity of vibration and the flow properties of the powder. Due to the design of the custom recoater, a homogenous temperature of the powder output could be achieved. Further, the vibrating blade system of the recoater system enables the processing of particle sizes slightly bigger than the layer thickness.
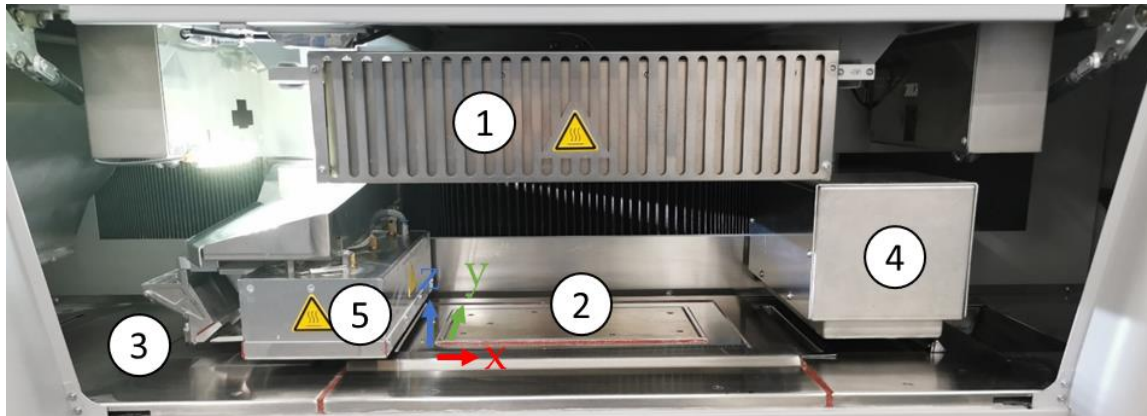

Figure 1: View of the build chamber of the voxeljet AG VX200 HSS: Overhead lamp ①, build box ②, recoater ③, printing module ④ and sintering lamp ⑤

The ink-printing module (④ in Figure 1), consisting of three XAAR 1003 print heads which are arranged staggered in two rows, was connected to the machine´s fluid circulation system. For manufacturing, the voxeljet AG HSS Ink Type B was used, containing carbon black as RAM. The sintering lamp (⑤ in Figure 1) was equipped with a 2kW halogen lamp. The selective energy input into the parts is determined by the combination of the speed and power of the sintering lamp and the amount of applied RAM.

Process Conditions

The parameters of Table 1 were used for manufacturing PEBA parts using HSS. The constants and variables used in this work are based on preliminary work on significant effects on HSS printed parts [6,7,14,24,31], machine specifications and experience values, providing a sound foundation of part properties. While the process temperature combined with the build box floor plate temperature determine the temperature level of the powder bed, the sintering lamp power, greyscale and sinter lamp speed determine the quantity and duration of the selective energy input. The greyscale value determines the amount of RAM that is applied per voxel (volume element) and thus the amount of energy that is induced into the polymer powder below. To evaluate the influence of the temperature level and the selective energy input into the parts, the process temperature (and build box floor plate temperature), the sintering lamp power, the sintering lamp speed and the greyscale were varied within the investigations using methods of Design of Experiments (DoE). The maximum and minimum sets of process parameters regarding the temperature level and selective energy input of this work´s framework were based on the conducted material analysis (DSC) and pretests with the VX200 HSS. Latter made it possible to assess tolerable thermal effects on the surface and sufficient mechanical properties of the HSS printed parts within the framework.

Table 1: Process parameters used for manufacturing PEBA specimens using HSS

Parameters	Values		
Constants			
Material	Evonik´s INFINAM TPA		
Powder ratio (used/virging)	70/30 %		
Temperature hysteresis	5 °C		
Build box wall temperature	90 °C		
Recoater temperature	60 °C		
Pre-sintering lamp power	0 %		
Overhead lamp power	28 %		
Recoater speed	0.1 m/s		
Ink print head speed	0.39 m/s		
Layer thickness	0.1 mm		
Recoater gap	3 mm		
Recoater vibration strength	100 %		
Pre-layers	40		
Post-layers	50		
Variables and Factors	Level 1	Level 2	Level 3
Process temperature (PT)	126°C	128°C	130°C
Build box floor plate temperature	126°C	128°C	130°C
Sintering lamp power (SLP)	65 %	70 %	75 %
Sintering lamp traverse speed (SLS)	0.20 m/s	0.21 m/s	0.22 m/s
Greyscale (GS)	1	3	5
	≙ 6 pL/voxel	≙ 18pL/voxel	≙ 30pL/voxel

A Definitive Screening design was used for the DoE. This particular choice of DoE with three levels for each factor was used to efficiently estimate main effects as well as quadratic terms, while minimizing the required number of experimental runs.

Table 2: Definitive screening experimental design and process parameters used for manufacturing PEBA parts by HSS

Experiment no.	SLP [%]	SLS [m/s]	PT [°C]	GS
1	65	0,20	126	5
2	65	0,20	130	5
3	65	0,22	130	1
4	70	0,21	128	3
5	75	0,21	130	1
6	65	0,20	128	1
7	70	0,20	126	1
8	75	0,22	128	5
9	65	0,22	126	3
10	65	0,21	126	5
11	75	0,22	126	1
12	75	0,20	126	5
13	75	0,20	130	3
14	70	0,22	130	5

While Table 1 provides detailed information about the four factors and their corresponding levels, Table 2 showcases the utilized DoE configuration. One set of parameters (experiment no. 1) was added to the DoE configuration to investigate the influence of the temperature level when compared with experiment no. 2. To analyse the Definitive Screening design, the software JMP Pro from JMP Statistical Discovery LLC was used. The main effects were analysed using standard least squares personality and a level of significance (p-value) of 0.05 (5%). Further, a prediction model was generated using the quadratic character of the definitive screening design to analyse the direction of improvement of part properties between the levels of each factor and to obtain an optimum set of parameters within the examined framework.

Layout, post-processing and analysis of the PEBA parts manufactured using HSS

The layout used for the experiments can be seen in Figure 2. The manufactured parts used in this work were the grey coloured six tensile bars (ISO 37 type 2), six density cuboids (17x17x10 mm) and two geometrical specimens to test the geometrical and dimensional accuracy. The latter have a cuboid shape as basis (37.5x30x10 mm), a cylindric hole with a diameter of 12 mm, inclined planes at angles of 15°, 30°, 45°, 60° and 75° and roundings with diameters of 5 mm, 6 mm and 7 mm following [32]. The height of the build job corresponds to 10 mm.
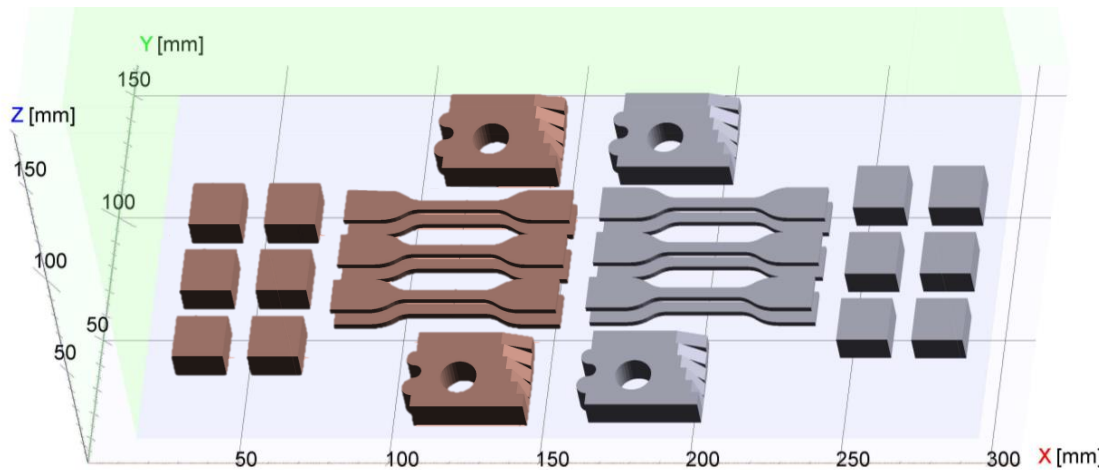

Figure 2: Layout of the build jobs containing two sets of specimens (coloured in red and grey): six tensile bars, six density cuboids and two geometrical specimens to test geometrical and dimensional accuracy

Tensile tests were done according to DIN ISO 37 using the tensile bars and a Zwick Roell Z1485 universal testing machine, a pre-load of 5 N and a testing speed for TPE parts according to DIN EN ISO/ASTM 52924 of 200 mm/min (1 mm/min for tensile modulus). Before testing, the tensile bars were conditioned within a Memmert UF55 fan oven according to DIN EN ISO 290 for 48 h at a temperature of 23°C and a relative humidity of 50%.

The density of the density cuboids was measured using Archimedes' principle according to DIN EN ISO 1183-1. By using a high-resolution scale Kern ALJ 160-4A, the weights of the samples were measured in air and subsequently within demineralised water with known density.

The density ρ_S of a cuboid was calculated with the mass of the cuboid in air $m_{S,A}$, the mass of the sample in the liquid $m_{S,IL}$ and the density of the liquid ρ_{IL} using equation 1. The density of demineralised water at a constant room temperature of 23 °C was $\rho_{IL}= 0.9976$ g/cm³.

$$\rho_S = \frac{m_{S,A} \times \rho_{IL}}{m_{S,A} \times m_{S,IL}} \text{ in g/cm}^3 \qquad\qquad equation\ 1$$

Hardness Shore A was measured using a Hildebrand HD3000 Durometer A according to DIN EN ISO 868. The central point of the top and bottom side of each of the density cuboids made from PEBA were used for the measurement of the hardness. It has to be mentioned, that the distance to each of the edges of the specimens of 12mm as required by DIN EN ISO 868 could not be ensured. For the analysis, an overall mean value Hardness Shore A of the six specimens (top and bottom surfaces included) was calculated.

Geometrical and dimensional accuracy was measured by optically 3D-scanning the geometrical specimens and comparing them against the individually scaled, original Computer-Aided Design (CAD) model. For this, a Carl Zeiss GOM Metrology GmbH 3D scanner ATOS Compact Scan 5M was used to create a scanned model of the geometric specimens and evaluate them with the corresponding software GOM Inspect 2022. The dimensions in x-, y- and z-direction of each scanned model of the geometric specimens were determined using the cuboid-shaped base. These three dimensions were then used to derive scaling factors for each geometric specimen before comparing the scanned model with the original CAD model. Each scanned model was subsequently scaled accordingly in the x-, y- and z-direction using Autodesk Inventor Professional 2020 software. This additional step is necessary to counter the influence of shrinkage that occurs during the cooldown phase of manufacturing in HSS, allowing for a comparison between the scanned model and an optimum CAD model with the same dimensions. After reimporting the scaled base model into GOM Inspect 2022, the volumes of the scanned and the CAD model were compared, computing the integrated absolute distance (variation in volume) in [mm³] for each specimen. For the analysis, a mean value of the variation in volume of the geometric sepecimens (top and bottom specimen) was calculated.

Results and Discussion

PEBA powder and particle size distribution

The measurements using pycnometry with helium gas showed a solid density ρ_F for virgin powder of 1.0477 ± 0.0004 g/cm³ (1.05 g/cm³) and 1.0616 ± 0.0008 (1.06 g/cm³) for used powder. The slightly higher density of the used powder compared to the virgin powder indicates a change on molecular level, e.g. a change in crystallinity, due to the exposure to elevated temperatures within the HSS process.

According to [33], a particle size distribution of approximately 20 to 80 µm and an aspect ratio (ratio of the smallest and largest diameter) of 1 of the particles is preferred for the HSS related AM process LS. Figure 3 shows the volume-based PSD curves of virgin and used PEBA powder. Virgin powder (Figure 3, left) shows, compared to used powder (Figure 3, right), a narrow but bimodal distribution with a pronounced peak at around 70 µm can be seen (d_{10}: 31.7 µm, d_{50}: 57.5 µm, d_{90}: 83.3 µm), being referring to Schmid appropriate for PBF-P processes. Only 2.02 % were bigger than the layer thickness of 100 µm. The used PEBA powder shows a broader, unimodal distribution which flattens out towards increasing particle sizes (d_{10}: 35.9 µm, d_{50}: 69.7 µm, d_{90}: 127.1 µm).
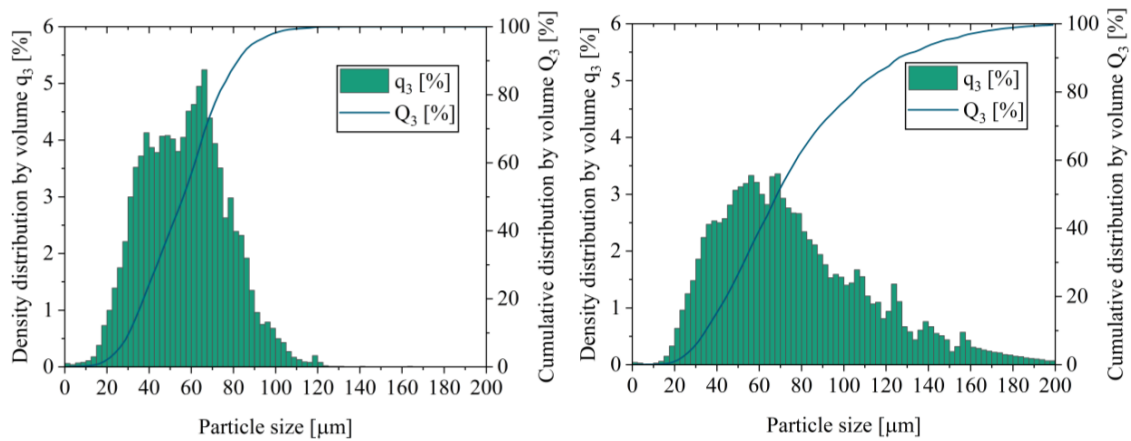
Figure 3: Volume-based particle size distribution of virgin PEBA powder (left) and used PEBA powder, sieved with 180 µm mesh (right). For the 180 µm sieved, used PEBA powder, 0.35 % of the particles were bigger than 200 µm.

The increase of the d_{10} and d_{50} values of used powder compared to virgin powder indicates an increase in particle size due to the exposure to elevated temperature levels within the HSS process and thermal induced sintering processes of the polymer particles. Despite sieving of the used powder through a 180 µm mesh sieve, 1.2 % of the particles are found to be bigger than 180 µm. This indicates the presence of particles with a low aspect ratio, which were able to pass through the sieve due to their small diameter. Despite these findings, the used mixture of PEBA powder with a ratio (used/virgin powder) of 70/30 demonstrated suitable powder flowability and a homogeneous powder bed surface.
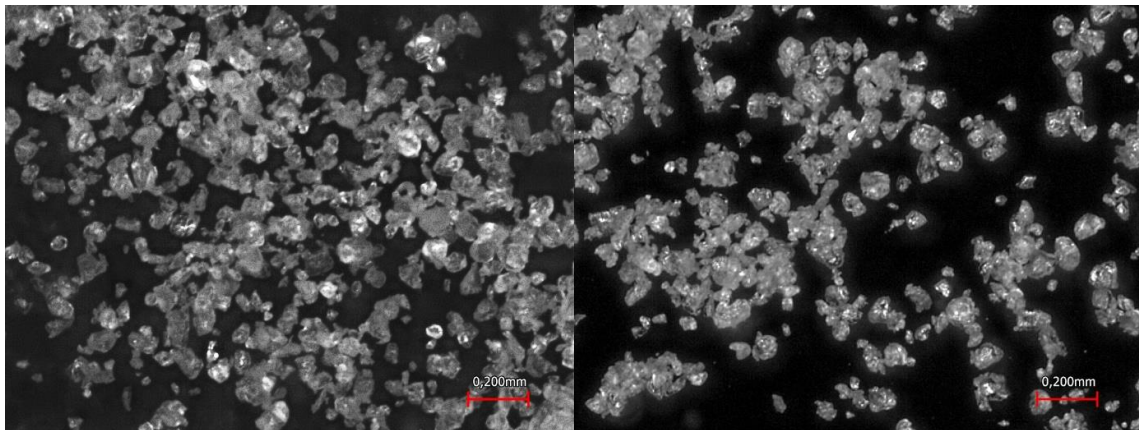

Figure 4: Microscopy images of virgin (left) and used (right) PEBA powder

Microscopy images of virgin and used PEBA powder (Figure 4) show an uniformly, potato-shaped particle form. The loss of small particle sizes can not be seen within the comparison of virgin and used powder. Nevertheless, used powder shows agglomerates of sintered polymer particles, which explains the unimodal distribution that flattens towards increasing particle sizes. The agglomeration of polymer particles, which can be seen in used PEBA powder also leads to particles of lower aspect ratio. Yet, no problems regarding powder flowability could be seen within the recoating process of the HSS with a mixture of PEBA powder with a ratio (used/virgin) of 70/30.

Figure 5 shows the heating and cooling curves of virgin PEBA powder. The melting peak shows a broad peak, which is flattening out towards decreasing temperatures. While the left

limit of the peak starts around 120°C, the melting onset temperature $T_{m,onset}$ of PEBA was determined at 131°C. This indicates thermal ageing of the polymer powder due to primal melting processes when processing temperatures of higher than 120°C are chosen. The cooling onset temperature $T_{c,onset}$ of PEBA was determined at 132°C.
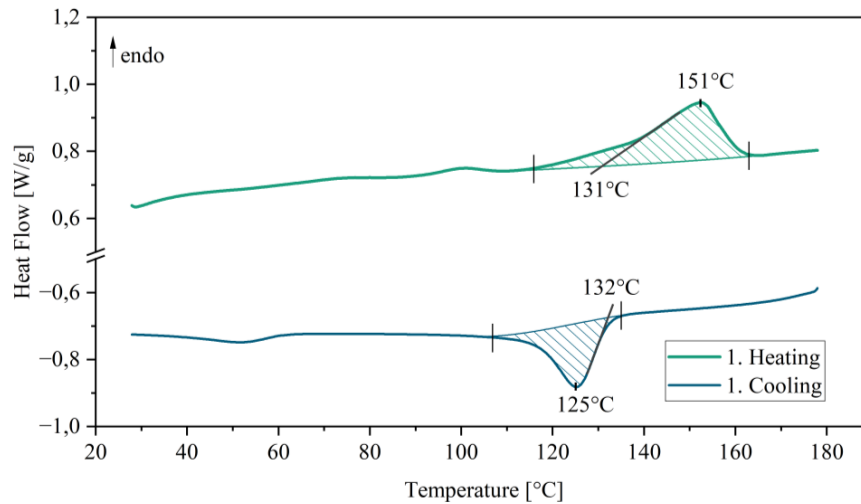

Figure 5: DSC of virgin PEBA powder. The top curve is the melting (endothermic) and the bottom curve is cooling (exothermic)

By subtracting $T_{c,onset}$ from $T_{m,onset}$, a negative sintering window of -1°C can be determined, indicating a low processability in PBF-P. Relating to the results of the DSC, a processing temperature higher than $T_{c,onset}$ should be used to avoid curling effects, which can lead to warping of the parts during the early layers of manufacturing and pull out effects of the powder bed by the recoater. In conflict with that, primal melting processes and thus thermal aging accompany as the process temperature exceeds $T_{m,onset}$. Comparing the melting enthalpy of the first (12.66 J/g) and second heating (11.94 J/g) of the PEBA powder, a small decrease in melting enthalpy was determined, indicating a decrease in crystallinity after full melting of the material. For used powder, a $T_{m,onset}$ of 134°C, a $T_{c,onset}$ of 131°C and thus a sintering window of 3°C was determined, which enhances the processability of the PEBA powder within the HSS process. Compared to the virgin powder, the melting enthalpy of the first heating of used PEBA powder decreased to 11.69 J/g, indicating, in contrary to the expectations from the solid density values, a small decrease in crystallinity. In the present investigations, no curling was obtained, even by using the lowest process temperature of 128°C. Further, unpacking of the parts from the loose, unsintered powder showed no increase in hardness of powder cake. This indicates an appropriate temperature level used for the experiments.

Definitive Screening Results

Table 3 shows the results of the previous introduced test methods using the HSS printed parts. The density value of experiment no. 4 was excluded within the analysis due to large deviation within the results of the prediction model of the analysis of the Definitive Screening design of experiments. Despite similar densities and hardness Shore A values, huge differences for tensile modulus, tensile strength, elongation at break and variation in volume can be identified. The parameter combination of high temperature level and high selective energy input of experiment no. 13 led to the highest density value of 1.02 g/cm³. By using the maximum reachable solid density of 1.06 g/cm³, this leads to a relative density of 96 %. It can be assumed that the low porosity of the parts of experiment no. 13 led to the highest mechanical properties, especially

regarding the value of elongation at break. In conflict with the high mechanical properties, the highest value of the variation in volume can be seen. Majewski et al. [6] and Norazman et al. [31] determined higher mechanical properties of HSS printed parts using higher PT, SLP and lower SLS, accompanied with an increase in hardness of the unsintered powder cake.

Figure 6: Front view of a geometrical specimen of the experiments13 (left) and experiment 3 (right)

It is assumed that a higher temperature level and selective energy input increases the variation in volume of HSS printed PEBA parts due to adhesion of unsintered polymer powder. Even after post processing using glass beed blasting, these adhesions can not be removed from the specimens, as can be seen in Figure 6.

Table 3: Results of the test methods used to analyse the HSS printed parts

Exp. no.	Density [g/cm³]	Tensile Modulus [MPa]	Tensile strength [MPa]	Elongation at break [%]	Hardness Shore A	Variation in volume [mm³]
1	1.00	77.38	6.05	38.39	87.20	359.40
2	1.01	81.43	6.49	54.59	87.50	381.70
3	0.91	65.99	4.29	24.12	84.70	302.30
4	(1.01)	82.22	6.41	49.40	87.70	350.80
5	0.96	82.76	5.71	41.52	87.50	308.10
6	0.91	66.83	4.28	24.93	85.20	370.70
7	0.90	62.08	3.94	23.57	85.00	390.40
8	1.01	82.76	6.58	54.49	88.00	358.20
9	0.97	75.80	5.22	27.73	87.40	391.60
10	1.00	84.60	5.87	28.01	87.50	365.20
11	0.93	69.97	4.66	25.61	84.60	373.00
12	1.01	85.20	6.76	57.54	87.40	376.20
13	1.02	89.46	7.19	86.17	88.00	428.40
14	1.01	88.48	6.81	53.92	87.40	347.80

Comparing experiments no. 1 and 2, where the effect of the process temperature can be analysed directly from the data of *Table 3*, it can be seen that tensile strength and elongation at break are improved by increasing PT from 126°C to 130°C, while the values of density, tensile modulus, hardness and variation in volume hardly increase.
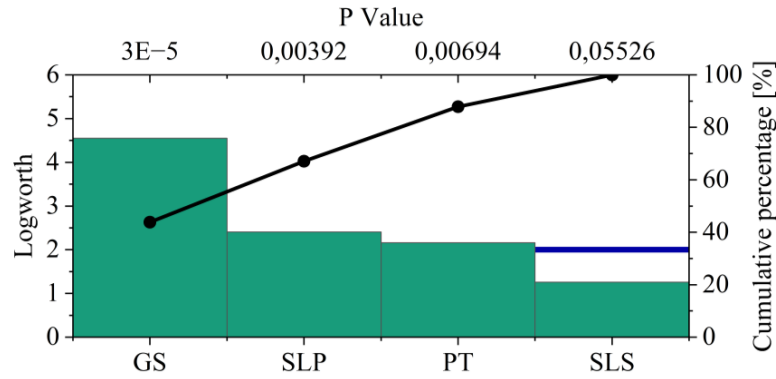
Figure 7: Pareto chart of the factors GS, SLP, PT and SLS

The main effects of the factors are plotted within a Pareto chart (Figure 7). The Logworth value is defined as -log10(P Value), where 2 is the threshold of significance. By comparing the P Values of SLP (0.00392) and PT (0.00694) with the level of significance of 0.05, PT and SLP have similar and significant effect on the overall part properties. By comparing the bar of the GS with SLP and PT, the variation of GS has the highest effect on overall part properties, being highly significant as $P \leq 0.001$. Comparing the bars of GS, SLP and PT, SLS has the least effect on overall part properties, since the $P > 0.05$.

To evaluate the effects of variation of the factors, a prediction model was generated using the definitive screening model and the linear regression of the standard least squares personality. Table 4 shows the model quality using the coefficient of determination R^2, which is a measure of the quality of the linear regression and ranges between 0 (low compliance) and 1 (high compliance). It can be seen that the prediction model possesses a high quality since most of the R^2 values are higher than 0.9. The lower, but still relatively high R^2 regarding variation in volume can be increased by an increase of the amount of analysed parts or an increase in experiments.

Table 4: Listing of the Model quality using the standard least squares personality and the coefficient of determination R^2

Target value	Density	Tensile modulus	Tensile strength	Elongation at break	Hardness Shore A	Variation in volume
Coefficient of determination R^2	0.99	0.96	0.98	0.99	0.94	0.80

A prediction analysis plot (Figure 8) was generated, where the effect of variation of the factors can be seen in relation to the target values density, tensile modulus, tensile strength, elongation at break, hardness Shore A and variation in volume. A quadratic prediction curve of GS can be seen, leading to an initial increase in mechanical properties with increasing the GS. Regarding elongation at break, hardness Shore A and variation in volume, a high level of GS leads to a decrease in properties, suggesting a saturation of absorbance at high GS. The more RAM is applied to the powder bed surface, the more synthetic carrier fluid is applied also. This leads to an energy loss of the selective energy input into the part due to the higher evaporation of the carrier fluid and potential residues of synthetic carrier fluid within the parts compared to low GS levels. Thus, an optimum in part properties can be expected at GS values of 3-4. An increase

in SLP and PT leads to an increase in overall part properties in an almost linear course. An increase of PT and SLP enhances sintering mechanisms and leads to higher density of the parts, which results in increased mechanical properties, density and hardness values.
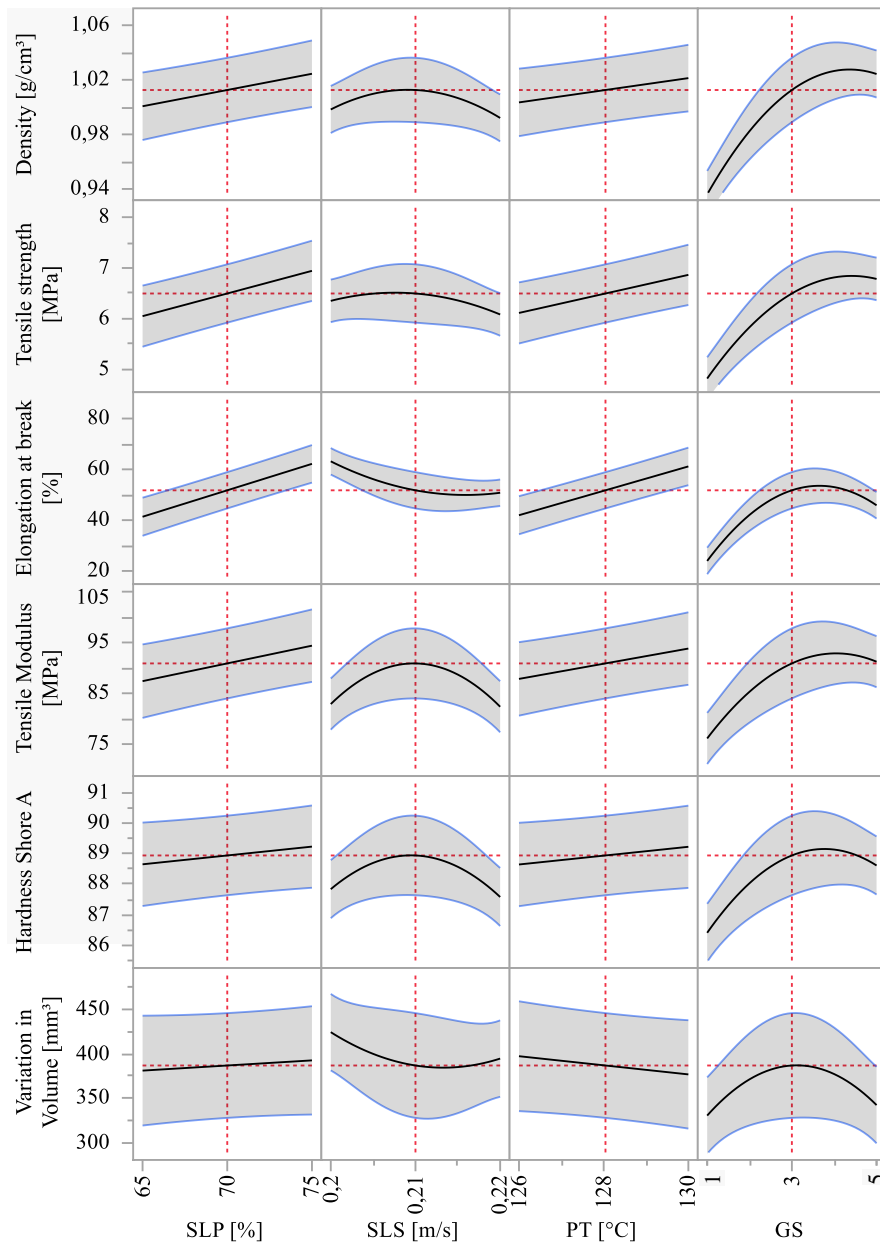

Figure 8: Prediction analysis plot of the definitive screening model

In contrary to that, lower power adhesion to the parts and thus a decrease in variation in volume is expected to be achieved by using a low temperature level of PT and low SLP. The non-significant factor SLS shows partially opposed prediction curves regarding mechanical properties. Curves of the target values in relation to SLS a parabolic behaviour. While for density, tensile modulus, tensile strength and hardness Shore A a maximum at 0.21 m/s is expected, elongation at break and variation in volume show a minimum at that level. Therefore, a SLS of 0.21 m/s is recommended within the framework of this work,

perpendicularly to the assumption of a low SLS leads to an to an increase in selective energy input into the parts, an increase in sintering and densification and thus an increase in mechanical properties. To increase the effect and significance of SLS on part properties, a higher range in levels should be used in further investigations, since SLS, in combination with SLP and GS, determines the essential selective energy input into HSS printed parts.

By adjusting the prediction model and desired part properties of the model, three parameter sets were predicted using the software JMP and an importance of each factor of 1. The first set focusses on maximizing the desirability of density, tensile modulus, tensile strength, elongation at break and Hardness Shore A, while minimizing the variation in volume, aiming to achieve maximum, overall part properties. The second set shared the same desirabilities as the first set, except for the exclusion of variation in volume, which was left unoptimized. This set focusses on maximum mechanical properties for applications with less emphasis on dimensional and geometrical accuracy. Lastly, the third set focusses on the dimensional and geometrical accuracy of HSS printed PEBA parts, regardless of their mechanical properties. In this case, the only target was to minimize the variation in volume. It has to be mentioned, that the maximized sets of parameters are local maximum values within the framework of this work´s investigations. The software JMP predicted parameter sets (Table 5) for maximum overall part properties (A), maximum mechanical properties (B) and minimum variation in volume (C) which can be used to manufacture parts directly or as a basis for further investigations and evaluation of global maximums for the target values.

Table 5: Predicted levels of the factors for optimised overall part properties, maximum mechanical properties and minimum variation in volume within this work´s framework

Parameter set	Factor			
	GS	SLP [%]	PT [°C]	SLS [m/s]
A	5	75	130	0.21
B	4	75	130	0.2
C	1	65	130	0.21

Parameter set	Target value					
	Density	Tensile Modulus	Tensile strength	Elongation at break	Hardness Shore A	Variation in volume
	[g/cm³]	[Mpa]	[Mpa]	[%]		[mm³]
A	1.04	97.64	7.60	65.48	89.18	337.13
B	1.03	91.22	7.45	86.00	88.62	414.85
C	0.93	74.65	4.65	21.47	86.22	312.22

Summary

In conclusion, this research focused on the processing of Polyether block amide (PEBA) powder using the High Speed Sintering (HSS) process in Additive Manufacturing. PEBA, a thermoplastic elastomer, offers high-performance characteristics such as high elasticity, low density, and high service temperature, making it an ideal material for applications in industries such as athletic footwear and outdoor equipment. This research focused specifically on the analysis of PEBA powder, its processability and the manufacturing of PEBA parts with HSS using varying process parameters.

The material analysis of PEBA powder revealed important characteristics regarding processability and part properties, such as solid density, particle form and size distribution and thermal behavior. Methods of Design of Experiments were employed to optimize the target values density, tensile modulus, tensile strength, elongation at break, hardness Shore A and variation in volume by varying the factors sinter lamp power, sinter lamp speed, process temperature and greyscale. A Definitive Screening design was used, which efficiently estimated main effects and quadratic terms while minimizing the number of experimental runs required. Based on the results of the material analysis and pretests, factor levels of this work´s framework of the Definitive Screening model were set. Tensile tests, density measurements, hardness Shore A tests, and 3D scanning were conducted to assess the performance of the parts.

The results of the experiments and analyses demonstrated the feasibility and potential of processing PEBA powder using the HSS process. The mechanical properties of the PEBA parts showed promising tensile strength and elastic behavior. The density measurements confirmed the effectiveness of the HSS process in achieving high-density parts. The hardness Shore A tests indicated the suitability of PEBA for various applications requiring different hardness levels using greyscale printing. The 3D scanning results revealed good geometrical and dimensional accuracy, demonstrating the capability of HSS to produce complex geometries with high precision. The generated prediction model of the Definitive Screening model was used to determine optimum sets of parameters for maximum overall part properties, maximum mechanical properties and minimum variation in volume within the examined framework.

Overall, this research contributes to the understanding and advancement of HSS as a viable additive manufacturing process for PEBA. The findings showcase the unique properties of PEBA and its potential in industries such as automotive, aerospace, sportswear, and medical applications. By expanding the range of materials available for HSS, this research opens up new opportunities for small to medium series production and paves the way for further investigations to optimise part properties for HSS printed PEBA parts. The successful processing of PEBA powder using the HSS process demonstrates the potential of this material and manufacturing technique, contributing to the continuous evolution of additive manufacturing and its applications.

References

[1] DIN EN ISO/ASTM 52900:2022-03, Additive Fertigung_- Grundlagen_- Terminologie (ISO/ASTM 52900:2021); Deutsche Fassung EN_ISO/ASTM 52900:2021, Beuth Verlag GmbH, Berlin.

[2] Handbook of Industrial Inkjet Printing, John Wiley & Sons, Ltd, 2017.

[3] Neil Hopkinson, Patrick J. Smith, Industrial 3D Inkjet Printing/Additive Manufacturing, in: Handbook of Industrial Inkjet Printing, John Wiley & Sons, Ltd, 2017, pp. 649–660.

[4] N. Hopkinson, P. Erasenthiran, High Speed Sintering - Early Research into a New Rapid Manufacturing Process, The University of Texas at Austin, 2004.

[5] H.R. Thomas, N. Hopkinson, P. Erasenthiran, High Speed Sintering – Continuing Research into a New Rapid Manufacturing Process, The University of Texas at Austin, 2006.

[6] C.E. Majewski, B.S. Hobbs, N. Hopkinson, Effect of bed temperature and infra-red lamp power on the mechanical properties of parts produced using high-speed sintering, Virtual and Physical Prototyping 2 (2007) 103–110. https://doi.org/10.1080/17452750701520915.

[7]   C.E. Majewski, D. Oduye, H.R. Thomas, N. Hopkinson, Effect of infra-red power level on the sintering behaviour in the high speed sintering process, Rapid Prototyping Journal 14 (2008) 155–160. https://doi.org/10.1108/13552540810878012.

[8]   M.J. Thompson, D.C. Whalley, N. Hopkinson, Investigating Dielectric Properties of Sintered Polymers for Rapid Manufacturing, The University of Texas at Austin, 2008.

[9]   H.R. Thomas, The construction and testing of an IR absorption metric for high speed sintering, 2010.

[10] M. Fahad, N. Hopkinson, Evaluation of Parts Produced by a Novel Additive Manufacturing Process, AMM 315 (2013) 63–67. https://doi.org/10.4028/www.scientific.net/AMM.315.63.

[11] A. Ellis, C.J. Noble, N. Hopkinson, High Speed Sintering: Assessing the influence of print density on microstructure and mechanical properties of nylon parts, Additive Manufacturing 1-4 (2014) 48–51. https://doi.org/10.1016/j.addma.2014.07.003.

[12] A. Ellis, C.J. Noble, L. Hartley, C. Lestrange, N. Hopkinson, C. Majewski, Materials for high speed sintering, J. Mater. Res. 29 (2014) 2080–2085. https://doi.org/10.1557/jmr.2014.156.

[13] F. Norazman, Realising the Potential of the High Speed Sintering Process for Industrial Implementation, 2018.

[14] C.J. Noble, A. Ellis, N. Hopkinson, Effect of Greyscale/Print Density on the Properties of High Speed Sintered Nylon 12, University of Texas at Austin, 2014.

[15] F. Norazman, P. Smith, N. Hopkinson, Spectral Analysis of Infrared Lamps for Use in the High Speed Sintering Process, University of Texas at Austin, 2016.

[16] D. Rouholamin, N. Hopkinson, Understanding the efficacy of micro-CT to analyse high speed sintering parts, Rapid Prototyping Journal 22 (2016) 152–161. https://doi.org/10.1108/RPJ-03-2014-0030.

[17] Z. Zhu, S. Lou, C. Majewski, Characterisation and correlation of areal surface texture with processing parameters and porosity of High Speed Sintered parts, Additive Manufacturing 36 (2020) 101402. https://doi.org/10.1016/j.addma.2020.101402.

[18] Z. Zhu, C. Majewski, Understanding pore formation and the effect on mechanical properties of High Speed Sintered polyamide-12 parts: A focus on energy input, Materials & Design 194 (2020) 108937. https://doi.org/10.1016/j.matdes.2020.108937.

[19] R.J. Williams, L. Fox, C. Majewski, The effect of powder age in high speed sintering of poly(propylene), RPJ 27 (2021) 707–719. https://doi.org/10.1108/RPJ-05-2020-0090.

[20] L. Fox, Investigation into the Use of Polypropylene in High Speed Sintering, 2019.

[21] A. Ellis, R. Brown, N. Hopkinson, The effect of build orientation and surface modification on mechanical properties of high speed sintered parts, Surf. Topogr.: Metrol. Prop. 3 (2015) 34005. https://doi.org/10.1088/2051-672x/3/3/034005.

[22] D. Pezold, M. Wimmer, F. Alfayez, Z. Bashir, F. Döpper, Evaluation of Polyethylene Terephthalate Powder in High Speed Sintering, Polymers 14 (2022) 2095. https://doi.org/10.3390/polym14102095.

[23] R. Brown, C.T. Morgan, C.E. Majewski, Not Just Nylon… Improving the Range of Materials for High Speed Sintering, University of Texas at Austin, 2018.

[24] A. Ellis, L. Hartley, N. Hopkinson, Effect of Print Density on the Properties of High Speed Sintered Elastomers, Metall Mater Trans A 46 (2015) 3883–3886. https://doi.org/10.1007/s11661-015-2833-4.

[25] Norazman, Farhana, et al, Smoother and stronger high speed sintered elastomers through surface modification process, International Journal of Rapid Manufacturing (2017) 155–169.

[26] J.S. Dick, C.P. Rader, Raw materials supply chain for rubber products: Overview of the global use of raw materials, polymers, compounding ingredients, and chemical intermediates, Hanser Publications, Cincinnati, 2014.

[27] U. Bruder, User's guide to plastic, secondnd edition, Hanser; Hanser Publications, Munich, Cincinnati, 2019.

[28] Rubber technology: compounding and testing for performance, 2020.

[29] E.A. Campo, Industrial Polymers, Hanser; Hanser Gardner, Munich, Cincinnati, Ohio, 2008.

[30] R.J. Williams, K.H. Al-Dirawi, R. Brown, J. Burt, A.E. Bayly, C. Majewski, Correlations between powder wettability and part colour in the High Speed Sintering process, Additive Manufacturing 47 (2021) 102361. https://doi.org/10.1016/j.addma.2021.102361.

[31] F. Norazman, N. Hopkinson, 2014. Effect of Sintering Parameters and Flow Agent on the Mechanical Properties of High Speed Sintered Elastomer. J. Manuf. Sci. Eng 136, 061006. https://doi.org/10.1115/1.4028482.

[32] Thomas Reinhardt, Entwicklung einer ganzheitlichen Verfahrenssystematik bei der Qualifizierung neuer Werkstoffe für das Laser-Sintern am Beispiel Polypropylen, 2016.

[33] M. Schmid, Laser sintering with plastics: Technology, processes, and materials, First edition, Hanser Publishers, Cincinnati, Munich, 2018.